SCIENCE CHINA
Chemistry

•ARTICLES•

August 2023 Vol.66 No.8: 2363–2370
https://doi.org/10.1007/s11426-023-1624-7

In-situ doping strategy for improving the photocatalytic hydrogen evolution performance of covalent triazine frameworks

Minghui Chen[1], Ji Xiong[1], Xiangyu Li[1], Quan Shi[1], Ting Li[1], Yaqing Feng[1,2,3] & Bao Zhang[1,2,3*]

[1]*School of Chemical Engineering and Technology, Tianjin University, Tianjin 300350, China;*
[2]*Collaborative Innovation Center of Chemical Science and Engineering (Tianjin), Tianjin 300072, China;*
[3]*Haihe Laboratory of Sustainable Chemical Transformations, Tianjin 300192, China*

Received February 15, 2023; accepted May 5, 2023; published online July 12, 2023

A highly conjugated network of covalent triazine frameworks (CTFs) on the one hand promotes light-harvesting, but on the other hand, also results in high carrier recombination which eventually limits their photocatalytic hydrogen evolution reaction (HER) rates. Thus, strategies to favorably tune the electronic configuration of CTFs for efficient photocatalytic HERs need to be developed, but still remain challenging. Herein, a simple *in-situ* defect strategy involving element doping is developed for the first time to introduce a heteroatom including S and Se into CTF-1 *via* the condensation of aldehydes with the mixture of the terephthalimidamide and the S- or Se-substituted terephthalimidamide under mild conditions. The doping content (*X*) is varied, resulting in a series of S- and Se-doped CTFs, named CTFS-1-*X* and CTFSe-1-*X*, respectively. Interestingly, for the S-doped CTFs, CTFS-1-10 shows the most excellent HER rate (4,992.3 μmol g^{-1} h^{-1}) from water splitting, while for the Se-doped ones, CTFSe-1-10 exhibits a photocatalytic HER rate of 5,792.8 μmol g^{-1} h^{-1}, both of which far surpass undoped CTFs (693.3 μmol g^{-1} h^{-1}). In-depth studies indicate that the introduction of S or Se atoms into CTFs could extend the light absorption and promote photo-generated electron-hole pairs migration. Meanwhile, S- or Se-doping could create heterogeneous electronic configuration in CTFs, which can help to suppress carrier recombination.

covalent triazine frameworks, heteroatom doping, hydrogen evolution

Citation: Chen M, Xiong J, Li X, Shi Q, Li T, Feng PY, Zhang PB. *In-situ* doping strategy for improving the photocatalytic hydrogen evolution performance of covalent triazine frameworks. *Sci China Chem*, 2023, 66: 2363–2370, https://doi.org/10.1007/s11426-023-1624-7

1 Introduction

With the energy crisis becoming serious, hydrogen has been regarded as one of the most promising green energy resources to replace traditional fossil fuels [1–3]. In recent years, the technique involving photocatalytic hydrogen evolution reactions (HERs) from water has been thus widely explored to attain hydrogen sustainably [4–6]. As a key component in this technique, various types of photocatalysts have been examined. Apart from the development of inorganic photocatalysts such as TiO_2 and CdS for photocatalytic water splitting [7–9], organic semiconductors have attracted more and more attention due to their rich varieties and readily tunable photophysical and photochemical properties.

As a class of promising organic semiconductors, porous conjugated polymers have witnessed enormous research interests [10] including porous carbon nitride (PCN) [11], porous organic polymers (POPs) [12], covalent triazine frameworks (CTFs) [13] and covalent organic frameworks (COFs) [14]. Among those, CTFs are featured with robust, highly conjugated and N-rich skeleton structures. Due to the presence of the strong built-in electric field between the donor (D) and the electron-poor triazine acceptor (A) motifs, the in-plane separation and transfer of photogenerated charges could be promoted. The triazine units in CTFs could

*Corresponding author (email: baozhang@tju.edu.cn)

also serve as the active sites for hydrogen evolutions [15]. Therefore, CTF photocatalysts have shown intensive potential in the visible-light-driven water splitting for hydrogen evolution [16–19].

Even though certain progress has been achieved for CTFs as photocatalysts in photocatalytic HERs, the HER rate is still limited and far from practical applications. It is believed that the highly conjugated network and the uniform distribution of D-A motifs throughout the skeleton of CTFs result in high carrier recombination rates which eventually influence the HER rate [20]. Strategies for suppressing carrier recombination have thus been reported. For example, Xu *et al*. [21] prepared a heterojunction between CTFs and inorganic metal oxides to facilitate the photo-generated charge separation and transfer from CTFs to the metal oxides for efficient photoelectrochemical water splitting. Zhang *et al*. [22,23] reported the construction of the asymmetric CTF containing four different D-A domains in the skeleton of CTFs and thus the uniform distribution of D-A motifs was broken leading to the suppressed carrier recombination and enhanced electron transfer. Other strategies involving the formation of anisotropic charge carrier migration pathways in the CTF plane were also developed [17,24,25], among which defect engineering *via* the element doping represents a promising and interesting one [26]. However, to the best of our knowledge, a mild *in-situ* defect strategy involving element doping has not been reported, and in particular, the doping elements are also limited [27].

The heteroatoms sulfur (S) and selenium (Se) have been widely explored as dopants in the photovoltaic fields [28,29]. Compared with the nitrogen atom in CTFs, these two elements are featured with lower electronegativities and greater atomic radii. Doping of S and Se into CTFs is expected to introduce electron-rich defects, which would break up the uniform distribution of D-A motifs in the skeleton and create anisotropic charge transport pathways. It is thus of interest to investigate how S- and Se-doping would tune the energy band gap, spin density and charge density in the doped-CTFs to eventually influence the light-harvesting and the photo-generated electron-hole separation and transportation. Furthermore, to maintain the high crystallinity of CTFs, a mild S- and Se-doping procedure also needs to be developed.

Herein, for the first time we report a mild *in-situ* defect engineering strategy for the S- and Se-doped CTF synthesis to efficiently tune the photocatalytic activities of CTF. As a proof of concept, the condensation of terephthaldehyde with the mixtures of terephthalimidamide and various amounts (*X* mol%) of thioterephthalamide or selenoterephthalamide resulted in the simple **CTF-1** (*X* = 0), **CTFS-1-*X*** (*X* = 5, 10, 15, 20) and **CTFSe-1-*X*** (*X* = 5, 10, 15, 20) under mild conditions (below 393.15 K and under air atmosphere). Interestingly, our results demonstrated that the S- and Se-doped **CTF-1** both exhibited an enlarged light absorption range and promoted charge transfer efficiency. Under the irradiation of visible light and in the presence of H_2PtCl_6 and triethanolamine (TEOA) as the sacrificial agent, for the S-doped CTFs, **CTFS-1-10** showed the most excellent HER rate (4,992.3 μmol g^{-1} h^{-1}) from water splitting, while for the Se-doped ones, **CTFSe-1-10** exhibited a photocatalytic HER rate of 5,792.8 μmol g^{-1} h^{-1}, both of which far surpassed the undoped CTFs (693.3 μmol g^{-1} h^{-1}). The best HER rates of the doped CTFs were approximately 7.3 and 8.2 times higher than that of the pristine CTF for **CTFS-1** and **CTFSe-1**, respectively. Detailed studies revealed that the introduction of heteroatom into frameworks *via* the developed mild condensation conditions could not only maintain the great crystallinity of CTFs, but efficiently tune the electronic configurations of CTFs. It is worth mentioning that because of distinctive electronegativities and atomic radii, Se atom seemed to be more capable of suppressing carrier recombination and promoting charge transfer than S atom. Overall, we developed a promising mild *in-situ* approach to synthesize S- and Se-doped CTFs, based on which the photogenerated carrier recombination can be efficiently suppressed, leading to the significantly improved photocatalytic water splitting performance for HERs.

2 Experimental

The synthesis methods for the monomer thioterephthalamide (**TBM**), selenoterephthalamide (**SBM**), the sulfur-doped model compound (**SDM**) and the selenium-doped model compound **(SeDM)** were summarized in the Supporting Information.

2.1 Synthesis of TBM and SBM

The monomer **TBM** was synthesized according to the literature approach [30]. The mixture of terephthalonitrile (2.0 mmol, 256 mg) and 10 mL DMF was stirred for 30 min under Ar. Then 2 M ammonium sulfide aqueous solution (15 mL) as the sulfur source was slowly added into the mixture and stirred at room temperature for another 12 h under Ar. The yielded yellow precipitate was collected by filtration and washed with 3×20 mL DMF and 3×20 mL water, separately. The collected powder was dried at room temperature under vacuum for 12 h to give a pale-yellow powder with an 87% yield. ^{1}H NMR (600 MHz, DMSO-d_6) δ 10.01 (s, 2H), 9.61 (d, J = 4.0 Hz, 2H), 7.86 (s, 4H).

The synthesis method of the monomer **SBM** was similar to that of **TBM**. Sodium hydrogen selenide in ethanol solution (2 M) was utilized as the selenium source. The final collected powder was dried at room temperature under vacuum for 12 h to give a dark red powder with a 93% yield. ^{1}H NMR (600 MHz, DMSO-d_6) δ 10.95 (s, 2H), 10.35 (d, J = 4.0 Hz, 2H), 7.84 (s, 4H).

2.2 Synthesis of CTFS-1-*X* and CTFSe-1-*X* (*X* = 5, 10, 15, 20)

The synthesis method of **CTFS-1-*X*** and **CTFSe-1-*X*** (*X* = 5, 10, 15, 20) was similar to that of the pristine **CTF-1**. The terephthaldehyde (172.7 mg, 1.0 mmol) and the mixed monomers (2.0 mmol, the mixture of *X* mol% **TBM** or **SBM** and (100-*X*) mol% terephthalimidamide dihydrochloride) were added into a three-necked flask equipped with a condenser. Cs_2CO_3 (586 mg, 2.2 mmol) was dispersed into the mixed solvent of dimethyl sulfoxide (DMSO) and water (*v*/*v* = 15:1, 32.0 mL) as the catalyst, which was added into the above flask. The reactants were then homogeneously heated at 60 °C for 12 h with continuous stirring. The mixture was gradually heated and kept at 80 °C for 12 h and 100 °C for another 12 h. Finally, the mixture was heated up to 120 °C and kept at this temperature for 72 h. After neutralization with aqueous HCl (3 M, 15 mL), the yellow solid was collected by filtration.

2.3 Photocatalytic performance test

Photocatalytic hydrogen evolution was conducted under visible light irradiation (≥420 nm) with the presence of 50 mg CTF, CTFS or CTFSe catalysts, 90 mL deionized water, 10 mL TEOA as the sacrificial agent and 3 wt% Pt as co-catalyst (obtained by the reduction of $H_2PtCl_6{\cdot}6H_2O$). The evolved gases were analyzed by gas chromatography and the apparent quantum efficiency (AQE) was obtained in the presence of 50 mg CTF catalysts under the light irradiation at 365, 450, 500 and 550 nm, respectively. The AQE was calculated by the following equation:

$$\mathrm{AQE}(\%) = \frac{2 \times \text{number of evolved } H_2 \text{ molecules}}{\text{number of incident photos}} \times 100\% = \frac{2 \times nN_A}{Pt \times \lambda / (hc)}$$

where *n* is moles of evolved H_2; N_A is the Avogadro constant; *P* is the light irradiation intensity, *t* is the irradiation time, *h* is the Plank constant and *c* is the light speed.

3 Results and discussion

3.1 The crystalline structure of CTFS-1-*X* and CTFSe-1-*X*

For the synthesis of S- and Se-doped CTFs, the terephthaldehyde and the mixture of terephthalimidamide dihydrochloride and various amounts (*X* mol%, *X* = 5, 10, 15, 20) of **TBM** or **SBM** in the mixed solvent of DMSO and water were heated below 393.15K and under air atmosphere in the presence of cesium carbonate as the catalyst, resulting the simple **CTFS-1-*X*** (*X* = 5, 10, 15, 20) and **CTFSe-1-*X*** (*X* = 5, 10, 15, 20) in good yields (Scheme 1). It is believed that during the condensation process, Schiff base formation occurred first, which cyclized with **TBM** or **SBM** with the loss of an ammonia molecule and subsequent oxidation using DMSO as an oxidant, leading to the S- or Se-doped triazine unit and the doped CTF skeleton (Scheme 1). As a representative, the **CTFS-1-10** and **CTFSe-1-10** would be discussed below and a detailed discussion of other materials with different doping contents could be found in the Supporting Information.

The crystalline structures of the pristine **CTF-1**, **CTFS-1-10** and **CTFSe-1-10** were obtained by powder X-ray diffraction (PXRD) analysis. As shown in Figure 1a, all three PXRD patterns of as-prepared CTFs exhibited similar two main diffraction peaks at 2θ = 7.2° and 25.35°, confirming that the obtained CTF material have the analogous ordered structure in the inner layers. The intensity of the XRD patterns for **CTFS-1-10** and **CTFSe-1-10** is only slightly lower than that of **CTF-1**, suggesting that the good crystallinity of the obtained CTFS and CTFSe materials could be maintained *via* this *in-situ* heteroatom-doped approach. It was interesting to observe that with the introduction of heteroatom S or Se (Figure 1a) and with the increasing amount of doped heteroatom (Figure S2, Supporting Information online), the (001) diffraction peak in the PXRD image shifted to the lower angle direction, indicating that the planarity of CTFs was weakened. These results could be due to the greater atomic radius of S or Se (compared with that of N), and the lower planarity of the S- or Se-doped triazine unit in the CTF skeleton.

The simulated PXRD pattern of the AA stacking mode (Figure 1a, b) in comparison with that of the AB stacking mode had more agreement with the experimental PXRD data. The simulated data of CTFs obtained by Materials Studio were shown in Figure S3. Interestingly, compared with the distance between the pristine **CTF-1** layers (3.486 Å), the distance between the **CTFS-1** or **CTFSe-1** layers was significantly increased (3.828 Å for **CTFS-1-10**, and 4.281 Å

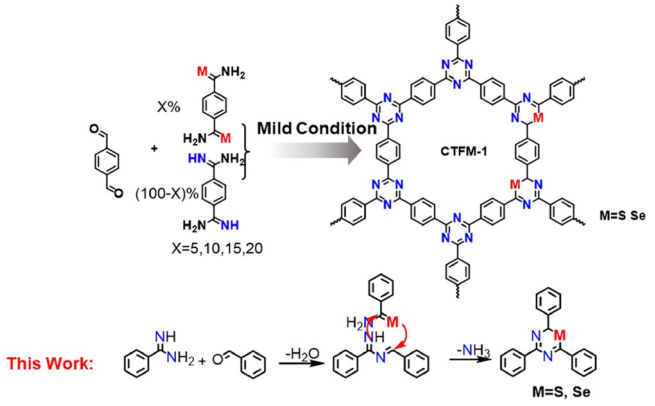

Scheme 1 Model reaction of synthesis of **CTF-1** and S- or Se-doped **CTF-1** (color online).

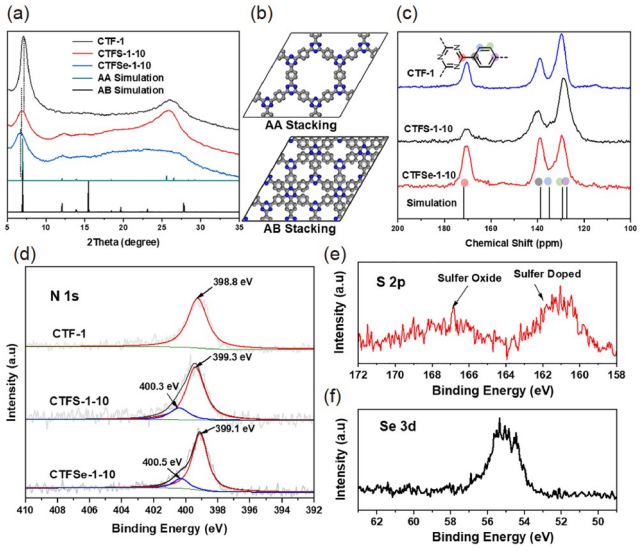

Figure 1 (a) The experimental PXRD of **CTF-1**, **CTFS-1-10** and **CTFSe-1-10**, compared with patterns simulated from structural models in the AA stacking mode (green line) and AB stacking mode (black line); (b) AA and AB stacking mode of **CTF-1**; (c) the solid ^{13}C NMR spectra of **CTF-1**, **CTFS-1-10** and **CTFSe-1-10**; (d) N 1s, (e) S 2p and (f) Se 3d high-resolution XPS spectra of **CTF-1**, **CTFS-1-10** and **CTFSe-1-10** (color online).

for **CTFSe-1-10**), implying that the π-π interaction between the 2D layers for the S- and Se-doped CTFs may be weakened. These could result from the decreased planarity of the S- and Se-doped CTFs, which is also demonstrated by the experimental PXRD results. The enlarged layer distance is expected to enable to suppress the photogenerated carrier recombination for the bulk materials to a certain extent [31].

Solid state ^{13}C nuclear magnetic resonance (NMR) spectra of **CTF-1**, **CTFS-1-10** and **CTFSe-1-10** verified the presence of the triazine units (173 ppm) and the benzene rings (138, 128 ppm), which fitted well with simulated data (Figure 1b). Fourier transform infrared spectra (FTIR) have been obtained to confirm the maintenance of conjugated backbone structures after heteroatom doping (Figure S4), in which the peaks at 1,510 and 1,355 cm^{-1} for **CTFS-1-10** or **CTFSe-1-10** were attributed to the presence of triazine units. However, due to the low doping amount of sulfur or selenium, signals ascribed to the bonding between carbon and sulfur or selenium were not observed. The results of the solid state ^{13}C NMR and FTIR analysis suggested that after sulfur or selenium doping, the chemical structures of **CTFS-1** and **CTFSe-1** were very similar to those of pristine **CTF-1**.

The pore structures of **CTFS-1-10**, **CTFSe-1-10** and **CTF-1** were evaluated by N_2 adsorption at 77 K and it was found that the specific surface area and pore volume of **CTF-1** were similar to those of S- or Se-doped **CTF-1**. **CTF-1**, **CTFS-1-10** and **CTFSe-1-10** all exhibited the type I N_2 isotherm (Figure S5), which revealed the main micropore characteristic with high Brunauer-Emmet-Teller (BET) surface areas.

Notably, the X-ray photoelectron spectroscopy (XPS) measurement provided further evidence of the presence of different doping element forms in the structures of **CTFS-1-10** and **CTFSe-1-10**. As shown in Figures S6b, c, the full survey XPS image showed that both frameworks, **CTFS-1-10** and **CTFSe-1-10**, contained C, N and O elements. The high-resolution N 1s surveys of **CTFS-1-10** and **CTFSe-1-10** displayed two contributing peaks deconvoluted by the main peaks, corresponding to triazine (C=N–C) at 399.3 eV and heteroatom-doped triazine units (C–S–C–N or C–Se–C–N) at 400.3 and 400.5 eV, respectively in Figure 1d. In comparison with the N 1s peaks of **CTF-1** (398.8 eV), those of **CTFS-1-10** and **CTFSe-1-10** shifted slightly towards a higher binding energy of 399.3 and 399.1 eV, respectively (Figure 1d), indicative of the influence of heteroatom doping on the electronic properties of the CTF skeleton.

The sulfur element could be found in the framework of **CTFS-1-10**, and selenium was found in **CTFSe-1-10**. According to the XPS survey, the atomic concentration of sulfur in **CTFS-1** was evaluated to be in a range of 0.5 mol%–2.7 mol% and selenium in **CTFSe-1** in a range of 0.3–2.2 mol% as shown in Table S2 (Supporting Information online). The detailed discussion could be found in the Supporting Information online. In the S 2p XPS high-resolution spectrum (Figure 1e), the main peak was centered at 161.2 eV, which was typical for C–S–C bond, suggesting that the C–S bond was successfully formed in **CTFS-1-10**. Similar results were observed in the Se 3d XPS high-resolution spectrum. As shown in Figure 1f, the main peak centered at 55.4 eV was assigned to the C–Se bond formed in **CTFSe-1-10**. These results also revealed that an S or Se atom was indeed covalently inserted into the triazine backbone.

Scanning electron microscopy (SEM) and transmission electron microscopy (TEM) were utilized to investigate the morphology of **CTF-1** and heteroatom-doped **CTF-1** shown in Figure 2. The SEM images of **CTF-1** suggested that the frameworks were synthesized featuring the layer structures (Figure S7). With the introduction and increasing amounts of S- or Se-doped into the frameworks, the surface of the layer was becoming less smooth (Figure S8) probably due to the reduced planarity of CTFs, which was expected to increase the interaction with the substrate. The TEM images also showed that the CTF materials were featured with compact layer structures (Figure 2g, h). As shown in Figure S9 and Figure 2c–f, the N, S and Se element distributions in **CTFS-1-10** and **CTFSe-1-10** could be obtained by X-ray energy dispersive spectrometer (EDS) analysis with the mapping scanning, respectively, which clearly demonstrated that the heteroatom was uniformly distributed within the frameworks, agreeing well with the results obtained from XPS analysis.

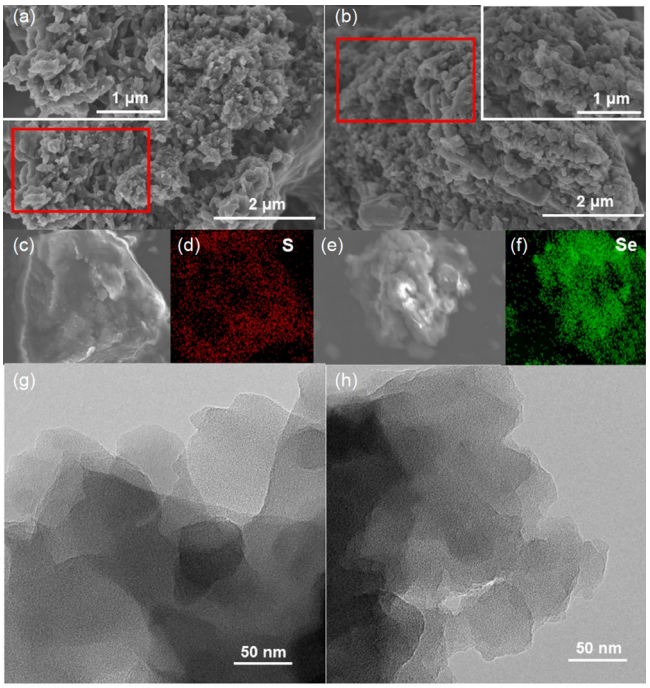

Figure 2 SEM images of (a) **CTFS-1-10** and (b) **CTFSe-1-10**. Inset: zoomed-in image within the annotated area. (c–f) Element mapping images of **CTFS-1-10** and **CTFSe-1-10**. (g, h) TEM Images of **CTFS-1-10** and **CTFSe-1-10** (color online).

3.2 The performance of photocatalytic hydrogen evolution

The photocatalytic performance for hydrogen evolution under visible light (>420 nm) using **CTF-1**, **CTFS-1** and **CTFSe-1** were evaluated in the presence of TEOA utilized as a sacrificial agent and 3 wt% Pt as a hydrogen evolving cocatalyst obtained by the reduction of $H_2PtCl_6{\cdot}6H_2O$. The photocatalytic conditions of HER have been optimized shown in Figure S10. It was revealed that along with the variation of the S- or Se-doping amounts, the trend of the HER rates for both **CTFS-1-*X*** and **CTFSe-1-*X*** (*X*=5, 10, 15, 20) showed an initial increase followed by a decrease. When the S- or Se-doping amounts reached 10 mol%, the hydrogen evolution of as-prepared **CTFS-1-10** and **CTFSe-1-10** could achieve the highest rate (249.6 and 286.5 μmol h^{-1}) under visible light irradiation, which was found to be 7.2 times and 8.3 times that of **CTF-1** (693.3 μmol g^{-1} h^{-1}). Interestingly, it was found that the HER performance of Se-doped CTFs was more efficient than that of S-doped materials, as shown in Figure S11.

Furthermore, the cyclic performance test of hydrogen evolution shown in Figure 3b suggested that the heteroatom-doped CTF materials could stably produce hydrogen by photocatalytic water splitting into 3 cycles. The materials also exhibited excellent durability and the efficient photocatalytic hydrogen evolution rate remained after 26 h irradiation. Moreover, the apparent quantum efficiency (AQE) of **CTF-1**, **CTFS-1-10** and **CTFSe-1-10** was obtained as shown in Figure S12. The maximum AQE of **CTFS-1-10** and **CTFSe-1-10** was measured up to 1.3% and 1.7% at 450 nm, respectively, both of which were higher than that of **CTF-1** (0.83%). The results also indicated that compared with the S element, the Se element introduced in the CTFs materials could promote the availability of single wavelength light and also play an important role in the full use of the light spectrum.

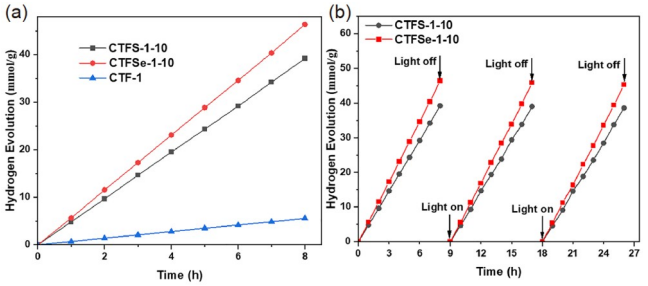

Figure 3 (a) The photocatalytic hydrogen evolution performance of **CTF-1**, **CTFS-1-10** and **CTFSe-1-10**; (b) the cyclic hydrogen evolution performance of **CTFS-1-10** and **CTFSe-1-10** (color online).

3.3 The mechanism of high photocatalytic activity

The photocatalytic HER performance investigated above indicated that the S- and Se-doping could effectively tune the electronic configuration and energy band structure of **CTF-1**. Thus, to further understand the role of S- and Se-doping in influencing the photocatalytic properties of CTF materials, the photophysical properties as well as the electronic band structures of **CTF-1**, **CTFS-1-10** and **CTFSe-1-10** were investigated by UV-vis DRS (Figure 4a). The detailed UV-vis DRS spectra of **CTFS-1-*X*** (*X* = 5, 15, 20) and **CTFSe-1-*X*** (*X* = 5, 15, 20) could be found in Figure S13. A red shift was observed for the absorption band edge of **CTFS-1-10** and **CTFSe-1-10**, compared with that of **CTF-1**, which demonstrated that the introduction of S and Se atoms into **CTF-1** enhanced the light absorption over the entire visible light range (700 nm≥λ≥420 nm) with the ideal visible spectrum efficiency reaching 52.3% (**CTFS-1-10**) and 59.7% (**CTFSe-1-10**), respectively, more than that of 42.6% for **CTF-1**. With the increasing of the doping content, the light absorption edge of both **CTFS-1-X** and **CTFSe-1-X** was extending from 550 to 670 nm, due to the introduction of sulfur or selenium into the framework.

All the Mott-Schottky plots of **CTF-1**, **CTFS-1-10** and **CTFSe-1-10** exhibited positive slopes at different frequencies in Figure S14, which featured a typical n-type semiconductor. The lowest unoccupied molecular orbital (LUMO) potential was very close to the flat band potential in the n-type semiconductor. Accordingly, the electrochemical Mott-Schottky plots exhibited that the LUMO potential of

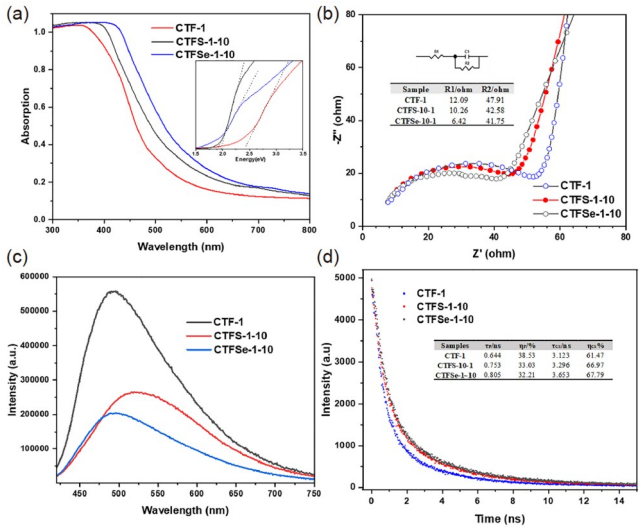

Figure 4 (a) The UV-vis diffuse reflection spectra of **CTF-1**, **CTFS-1-10** and **CTFSe-1-10** powers. Inset: plot of Kubelka-Munk function *versus* the energy of **CTF-1**, **CTFS-1-10** and **CTFSe-1-10**. (b) EIS Nyquist plots of **CTF-1**, **CTFS-1-10** and **CTFSe-1-10**. (c) Room-temperature PL emission spectra of **CTF-1**, **CTFS-1-10** and **CTFSe-1-10**. (d) Transient fluorescence lifetime of **CTF-1**, **CTFS-1-10** and **CTFSe-1-10** (color online).

CTF-1, **CTFS-1-10** and **CTFSe-1-10** were at approximately −1.19, −1.24 and −1.28 V *versus* the saturated Ag/AgCl reference electrode, respectively, in Figure S14. The results indicated that for all three CTF materials, the photocatalytic HERs *via* water splitting could occur thermodynamically. The more negative LUMO potentials for **CTFS-1-10** and **CTFSe-1-10** indicated that S- and Se-doping could significantly enhance the photo reducibility of **CTF-1** materials, which would be beneficial for photocatalytic water splitting. As illustrated in Figure 4b, the electrochemical impedance spectroscopy (EIS) measurement showed that obviously the diameters of arc radii of both **CTFS-1-10** (41.75 Ω) and **CTFSe-1-10** (42.58 Ω) were smaller than that of **CTF-1** (47.91 Ω), indicating that recombination of the photogenerated carriers was suppressed after the dopant introduction.

Furthermore, the photoluminescence (PL) measurement could provide a useful tool to evaluate the separation and migration of photoinduced electron-hole pairs, which were regarded as the basic processes in photocatalytic reactions. The fluorescence emission spectra of **CTF-1**, **CTFS-1-10** and **CTFSe-1-10** in the range 400–750 nm were shown in Figure 4c. **CTF-1** sample displayed higher PL intensity with respect to **CTFS-1-10** and **CTFSe-1-10**, indicating that the introduction of S or Se could promote the separation and migration of photoinduced carriers. It was further found that all the time-resolved fluorescence of **CTF-1**, **CTFS-1-10** and **CTFSe-1-10** followed a biexponential decay function (Figure 4d). The longer components (charge separation time) were calculated to be 3.123 ns for **CTF-1**, 3.296 ns for **CTFS-1-10** and 3.653 ns for **CTFSe-1-10**, and the charge combination lifetimes as shorter components of **CTF-1**, **CTFS-1-10** and **CTFSe-1-10** fitted to be 0.644, 0.753 and 0.805 ns, respectively. The results indicated that the introduction of S or Se into the CTFs could promote charge migration and restrain the recombination of charge carriers.

To further elucidate the influence of S or Se substitution for an N atom in the triazine ring on the charge transfer properties of the CTF skeleton, the change of the built-in electric field in the CTF materials before and after doping could be primarily considered. It has been reported that there is a positive correlation between the zeta and surface potentials of the CTF materials and the intensity of the built-in electric field [32]. As shown in Figure S15, the zeta potential of **CTFSe-1-10** could reach 27.4 mV, which was larger than those of **CTFS-1-10** (25.1 mV) and **CTF-1** (17.3 mV). The surface potential results obtained by the Kelvin probe force microscope (KPFM) in Figure S16 showed that the potential value of **CTFSe-1-10** (ΔE=123.1 mV) was also greater than those of **CTFS-1-10** (ΔE=112.4 mV) and **CTF-1** (ΔE=53.2 mV). These results indicated that the stronger built-in electric field could be a result of doping S or Se elements into **CTF-1** materials. The **CTFSe-1** was supposed to possess the strongest built-in electric field among the three CTF materials. Furthermore, the intensity of the built-in electric field could also be related to the surface charge density of 2D materials, which could be evaluated from the transient photocurrent density. As indicated in Figure S17, the surface charge density of **CTFSe-1-10** was estimated to be 1.73 times and 3.72 times as high as that of **CTFS-1-10** and **CTF-1**, respectively. **CTFS-1-10** and **CTFSe-1-10** also exhibited the highest photocurrent among all the doped **CTF-1** materials with various amounts of S and Se introduced, respectively, under visible light irradiation, indicating that the **CTFS-1-10** and **CTFSe-1-10** with the optimal amount of S or Se dopant (10 mol%) could realize the highest charge-transfer and separation efficiency.

To further demonstrate the electron-transfer process in **CTF-1** after introduction of heteroatom into the triazine ring, density functional theory (DFT) calculations with the B3LYP/6-31G(d) basis set in Gaussian 16 package were applied to optimize ground-state structures of the cluster model, triphenyltriazine named **SBM**, S-substituted triphenyltriazine named **SDM** and Se-substituted triphenyltriazine named **SeDM**, and to calculate the molecular orbitals and the electrostatic potential distribution as shown in Figure 5 and Figures S17c–S19. In comparison with **SBM** (−9.32 kcal/mol), the electrostatic potential of triazine unit in **SDM** (−11.41 kcal/mol) and **SeDM** (−12.37 kcal/mol) have become more negative, which indicated that the triazine units in **SDM** and **SeDM** could provide more photogenerated electrons utilized for water splitting after photoexcitation. Besides, according to Figure 5b, the theoretical energy levels were calculated

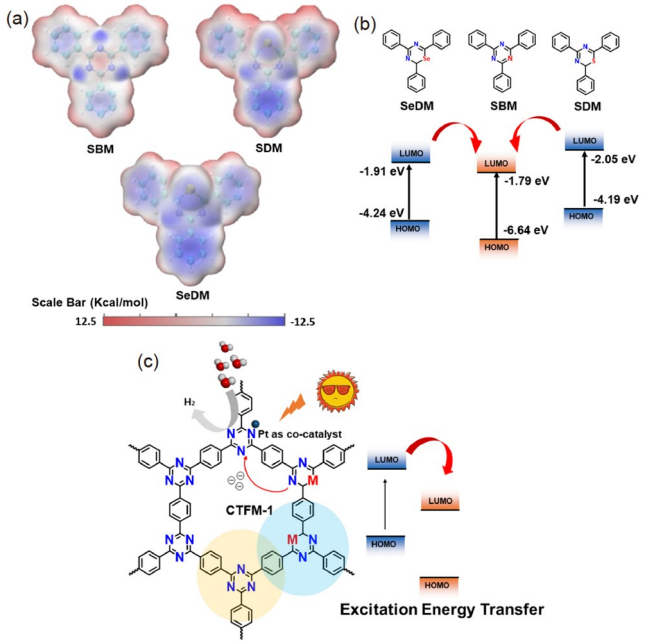

Figure 5 (a) The electrostatic potential distribution of **SBM**, **SDM** and **SeDM**. (b) The theoretical HOMO and LUMO orbits of **SBM**, **SDM** and **SeDM**. (c) The photocatalytic mechanism of heteroatom-doped **CTF-1** (color online).

based on the structural model of **SBM**, **SDM** and **SeDM**. The highest occupied molecular orbital (HOMO) and LUMO potentials of the structural model were shown in Figure 5b. Compared with the LUMO potential of **SBM** (−1.79 eV), those of **SDM** (−2.05 eV) and **SeDM** (−1.91 eV) were more negative, and the band gaps for **SDM** (2.14 eV) and **SeDM** (2.33 eV) lower than that of **SBM** (4.85 eV). The theoretical calculation results indicated that the excitation energy transfer (EET) could occur from **SDM** or **SeDM** to **SBM**, which could inhibit the carrier combination to enhance photocatalytic efficiency.

Based on the above analysis, we thus proposed the photocatalytic mechanism for heteroatom-doped **CTF-1** as shown in Figure 5c. Upon visible-light irradiation, the catalyst could be excited. The built-in electric field facilitated the charge transfer from the benzene units and doped triazine units to the triazine *via* the D-A and EET structure, which promoted photogenerated electrons to participate in the reduction reaction with the presence of Pt as the co-catalyst and triethanolamine as the sacrificial agent.

4 Conclusions

In summary, the novel facile approach for the *in-situ* preparation of heteroatom-doped (including S and Se element) CTFs has been developed. S or Se atoms were introduced into the triazine frameworks through thermal condensation between the aldehyde monomer and the mixture of terephthalimidamide and S or Se substituted terephthalamide, respectively. The highly crystalline and conjugated structure was maintained after the incorporation of S or Se into the frameworks of CTF-1. S- and Se-doped CTFs showed outstanding photocatalytic HER performance under visible radiation. When the amounts of S- or Se-substituted terephthalamide reached 10 mol%, the greatest photocatalytic hydrogen evolution rate of **CTFS-1-10** (4,992.3 μmol g^{-1} h^{-1}) and **CTFSe-1-10** (5,792.8 μmol g^{-1} h^{-1}) was achieved. It is shown that the introduction of heteroatom into frameworks *via* these mild condensation conditions could efficiently tune the electronic structures of CTFs. Overall, this work developed a simple and facile method for the synthesis of conjugated heteroatom-doped polymer semiconductors with highly efficient photocatalytic water-splitting capabilities. Our studies actually opened a gate toward the facile and efficient tuning of the electronic configuration of CTFs for highly crystalline and high-performance CTF photocatalysts.

Acknowledgements This work was supported by the National Natural Science Foundation of China (22078241), and the Fundamental Research Funds for the Central Universities and the Haihe Laboratory of Sustainable Chemical Transformations.

Conflict of interest The authors declare no conflict of interest.

Supporting information The supporting information is available online at chem.scichina.com and link.springer.com/journal/11426. The supporting materials are published as submitted, without typesetting or editing. The responsibility for scientific accuracy and content remains entirely with the authors.

1 Park JM, Lee JH, Jang WD. *Coord Chem Rev*, 2020, 407: 213157
2 Pan H. *Renew Sustain Energy Rev*, 2016, 57: 584–601
3 Younis SA, Kwon EE, Qasim M, Kim KH, Kim T, Kukkar D, Dou X, Ali I. *Prog Energy Combust Sci*, 2020, 81: 100870
4 Hisatomi T, Domen K. *Nat Catal*, 2019, 2: 387–399
5 Xu Q, Zhang L, Cheng B, Fan J, Yu J. *Chem*, 2020, 6: 1543–1559
6 Wang Y, Vogel A, Sachs M, Sprick RS, Wilbraham L, Moniz SJA, Godin R, Zwijnenburg MA, Durrant JR, Cooper AI, Tang J. *Nat Energy*, 2019, 4: 746–760
7 Gao J, Xue J, Jia S, Shen Q, Zhang X, Jia H, Liu X, Li Q, Wu Y. *ACS Appl Mater Interfaces*, 2021, 13: 18758–18771
8 She H, Sun Y, Li S, Huang J, Wang L, Zhu G, Wang Q. *Appl Catal B-Environ*, 2019, 245: 439–447
9 Zhang C, Xie C, Gao Y, Tao X, Ding C, Fan F, Jiang H. *Angew Chem*, 2022, 134:
10 Chen M, Li H, Liu C, Liu J, Feng Y, Wee AGH, Zhang B. *Coord Chem Rev*, 2021, 435: 213778
11 Zhang G, Liu M, Heil T, Zafeiratos S, Savateev A, Antonietti M, Wang X. *Angew Chem Int Ed*, 2019, 58: 14950–14954
12 Zhao C, Chen Z, Shi R, Yang X, Zhang T. *Adv Mater*, 2020, 32: 1907296
13 Wang N, Cheng G, Guo L, Tan B, Jin S. *Adv Funct Mater*, 2019, 29: 1904781
14 Wang X, Chen L, Chong SY, Little MA, Wu Y, Zhu WH, Clowes R, Yan Y, Zwijnenburg MA, Sprick RS, Cooper AI. *Nat Chem*, 2018, 10: 1180–1189

15 Zhai L, Xie Z, Cui CX, Yang X, Xu Q, Ke X, Liu M, Qu LB, Chen X, Mi L. *Chem Mater*, 2022, 34: 5232–5240
16 Liu M, Jiang K, Ding X, Wang S, Zhang C, Liu J, Zhan Z, Cheng G, Li B, Chen H, Jin S, Tan B. *Adv Mater*, 2019, 31: 1807865
17 Huang W, He Q, Hu Y, Li Y. *Angew Chem Int Ed*, 2019, 58: 8676–8680
18 Huang W, Wang ZJ, Ma BC, Ghasimi S, Gehrig D, Laquai F, Landfester K, Zhang KAI. *J Mater Chem A*, 2016, 4: 7555–7559
19 Schwinghammer K, Hug S, Mesch MB, Senker J, Lotsch BV. *Energy Environ Sci*, 2015, 8: 3345–3353
20 Cao S, Li H, Tong T, Chen HC, Yu A, Yu J, Chen HM. *Adv Funct Mater*, 2018, 28: 1802169–1802177
21 Zhang Y, Lv H, Zhang Z, Wang L, Wu X, Xu H. *Adv Mater*, 2021, 33: 2008264
22 Huang W, Byun J, Rörich I, Ramanan C, Blom PWM, Lu H, Wang D, Caire da Silva L, Li R, Wang L, Landfester K, Zhang KAI. *Angew Chem Int Ed*, 2018, 57: 8316–8320
23 Cheng H, Lv H, Cheng J, Wang L, Wu X, Xu H. *Adv Mater*, 2022, 34: 2107480
24 Zhang G, Zhang M, Ye X, Qiu X, Lin S, Wang X. *Adv Mater*, 2014, 26: 805–809
25 Kong D, Han X, Xie J, Ruan Q, Windle CD, Gadipelli S, Shen K, Bai Z, Guo Z, Tang J. *ACS Catal*, 2019, 9: 7697–7707
26 Kurumisawa Y, Higashino T, Nimura S, Tsuji Y, Iiyama H, Imahori H. *J Am Chem Soc*, 2019, 141: 9910–9919
27 Zhou N, Prabakaran K, Lee B, Chang SH, Harutyunyan B, Guo P, Butler MR, Timalsina A, Bedzyk MJ, Ratner MA, Vegiraju S, Yau S, Wu CG, Chang RPH, Facchetti A, Chen MC, Marks TJ. *J Am Chem Soc*, 2015, 137: 4414–4423
28 Ma X, Tang C, Ma Y, Zhu X, Wang J, Gao J, Xu C, Wang Y, Zhang J, Zheng Q, Zhang F. *ACS Appl Mater Interfaces*, 2021, 13: 57684–57692
29 Li S, Yang Y, Su K, Zhang B, Feng Y. *Chin J Chem Eng*, 2022, 50: 29–42
30 Zhang Y, Mori T, Ye J, Antonietti M. *J Am Chem Soc*, 2010, 132: 6294–6295
31 Wang K, Yang LM, Wang X, Guo L, Cheng G, Zhang C, Jin S, Tan B, Cooper A. *Angew Chem Int Ed*, 2017, 56: 14149–14153
32 Jing J, Yang J, Zhang Z, Zhu Y. *Adv Energy Mater*, 2021, 11: 2101392